International Journal of Thermophysics, Vol. 24, No. 2, March 2003 (© 2003)

The Validity of Using the Microscopic Hyperbolic Heat Conduction Model Under a Harmonic Fluctuating Boundary Heating Source

M. Naji,[1] M. A. Al-Nimr,[1, 2] and M. Hader[1]

Received August 1, 2002

The validity of using the microscopic hyperbolic heat conduction model under a harmonic fluctuating boundary heating source is investigated. It is found that using the microscopic hyperbolic heat conduction model is essential when $\frac{\bar{\omega}C_l}{G} > 0.1$. The phase shift between the electron-gas and solid-lattice temperatures is found to be $\tan^{-1}(\frac{\bar{\omega}C_l}{G})$. This phase shift reaches a fixed value of 1.5708 rad at very large values of $\frac{\bar{\omega}C_l}{G}$. It is found that the use of the microscopic hyperbolic heat conduction model is essential when $\bar{\omega} > 1 \times 10^9$ rad·s^{-1} for most metallic layers independent of their thickness.

KEY WORDS: hyperbolic microscopic model; hyperbolic two-step heat conduction model; macroscopic heat conduction; microscopic heat conduction; two-step heat conduction model.

1. INTRODUCTION

Energy transport during high-rate heating of thin metal films is a rapidly emerging area in heat transfer [1–15]. When a thin film is exposed to a very rapid heating process, such as that induced by a short-pulse laser, the typical response time for the film is on the order of picoseconds, which is comparable to the phonon-electron thermal relaxation time. Under these conditions, thermal equilibrium between the solid lattice and electron gas cannot be assumed and heat transfer in the electron gas and the metal lattice needs to be considered separately. Models describing the nonequilibrium thermal behavior in such cases are called the microscopic two-step models. Two microscopic heat conduction models are available in the

[1] Mechanical Engineering Department, Jordan University of Science and Technology, P.O. Box 3030, Irbid 22110, Jordan.

[2] To whom correspondence should be addressed. E-mail: malnimr@just.edu.jo

0195-928X/03/0300-0545/0 © 2003 Plenum Publishing Corporation

literature. The first one is the parabolic two-step model [1–5, 8–10] and the second one is the hyperbolic two-step model [1, 3, 7, 11].

Ultrafast heating of metals consists of two major steps of energy transfer that occur simultaneously. In the first step, electrons absorb most of the incident radiation energy and the excited electron gas transmits its energy to the lattice through the inelastic electron-phonon scattering process [1, 3]. In the second step, the incident radiation absorbed by the metal film diffuses spatially within the film mainly by the electron gas. For typical metals, depending on the degree of electron-phonon coupling, it takes about 0.1 to 1 ps for electrons and lattice to reach thermal equilibrium. When the ultrafast heating pulse duration is comparable with or less than this thermalization time, electrons and lattice are not in thermal equilibrium.

In the literature, numerous studies have been conducted using the microscopic hyperbolic heat conduction model [1, 3, 7, 11]. These studies show that the use of this model is a necessity in applications involving very thin films and very short duration heating sources. In the present work, we intend to investigate the thermal behavior of metal films under the effect of a harmonic fluctuating heating source applied at the film boundary and as described by the hyperbolic microscopic heat conduction model. The heating source will heat the electron gas, which in turn exchanges part of its energy with the solid lattice. In applications involving heating sources with very high frequency, there is not enough time available for the electron gas and solid lattice to attain the same temperature. The goal of the present work is to investigate the conditions under which the use of the microscopic hyperbolic heat conduction model is a necessity.

2. ANALYSIS

Consider a plate of thickness $2L$ where the boundaries of the plate are subjected to an imposed temperature that fluctuates in a harmonic manner and the origin of the x-axis is attached at the plate center. The frequency of fluctuations is very high so that the use of the microscopic heat conduction model becomes important. The governing equations describing the film thermal behaviour under these conditions are given as [1]

$$C_e \frac{\partial T_e}{\partial t} = -\frac{\partial q}{\partial x} - G(T_e - T_l) \tag{1}$$

$$C_l \frac{\partial T_l}{\partial t} = G(T_e - T_l) \tag{2}$$

$$\tau_F \frac{\partial q}{\partial t} + k_e \frac{\partial T_e}{\partial x} + q = 0 \tag{3}$$

The boundary conditions are given as

$$\frac{\partial T_e}{\partial x}(t, 0) = 0, \qquad T_e(t, L) = T_o(1 + \varepsilon \sin \bar{\omega} t) \tag{4}$$

where ε and $\bar{\omega}$ are, respectively, the amplitude and angular velocity of the fluctuating temperature imposed on the boundaries.

Now using the dimensionless parameters defined in the nomenclature, Eqs. (1) to (4) are reduced to

$$\frac{\partial \theta_e}{\partial \eta} = -\frac{\partial Q}{\partial \zeta} - A(\theta_e - \theta_L) \tag{5}$$

$$\frac{\partial \theta_l}{\partial \eta} = AC_R(\theta_e - \theta_l) \tag{6}$$

$$\frac{\partial Q}{\partial \eta} + B\frac{\partial \theta_e}{\partial \zeta} + Q = 0 \tag{7}$$

$$\frac{\partial \theta_e}{\partial \zeta}(\eta, 0) = 0, \qquad \theta_e(\eta, 1) = \varepsilon \sin \omega\eta = \varepsilon \operatorname{Im}\{e^{i\omega\eta}\} \tag{8}$$

where Im refers to "the imaginary part of" and i is the imaginary number $\sqrt{-1}$. Also,

$$A = \frac{G\tau_F}{C_e}, \qquad B = \frac{k_e \tau_F}{L^2 C_e}, \qquad C_R = \frac{C_e}{C_l}$$

$$Q = \frac{q\tau_F}{LC_e T_o}, \qquad \omega = \bar{\omega}\tau_F$$

Equations (5) to (8) assume solutions in the form:

$$\begin{aligned} \theta_e(\eta, \zeta) &= \operatorname{Im}\{W_e(\zeta)\, e^{i\omega\eta}\} \\ \theta_l(\eta, \zeta) &= \operatorname{Im}\{W_l(\zeta)\, e^{i\omega\eta}\} \\ Q(\eta, \zeta) &= \operatorname{Im}\{E(\zeta)\, e^{i\omega\eta}\} \end{aligned} \tag{9}$$

Substitution of Eq. (9) into Eqs. (5) to (8) yields

$$i\omega W_e = -\frac{dE}{d\zeta} - A(W_e - W_l) \tag{10}$$

$$i\omega W_l = AC_R(W_e - W_l) \tag{11}$$

$$i\omega E + B\frac{dW_e}{d\zeta} + E = 0 \tag{12}$$

$$\frac{dW_e}{d\zeta}(0) = 0, \qquad W_e(1) = \varepsilon \tag{13}$$

Equations (10) to (13) are decoupled and solved to yield

$$W_e(\zeta) = \varepsilon \frac{\cosh \lambda\zeta}{\cosh \lambda} \tag{14}$$

$$W_l(\zeta) = M\varepsilon \frac{\cosh \lambda\zeta}{\cosh \lambda} \tag{15}$$

$$E(\zeta) = -\frac{B\varepsilon}{1+i\omega}\lambda \frac{\sinh \lambda\zeta}{\cosh \lambda} \tag{16}$$

with

$$M = \frac{C_R A}{i\omega + C_R A} \tag{17}$$

and

$$\lambda = \sqrt{\frac{(1+i\omega)}{B}(A + i\omega - AM)}$$

Equation (17) may be rewritten as

$$M = \frac{C_R A}{\sqrt{\omega^2 + C_R^2 A^2}} e^{-i\delta} \tag{18}$$

with

$$\delta = \tan^{-1}\left(\frac{\omega}{C_R A}\right) \tag{19}$$

where δ represents the phase shift between electron-gas and solid-lattice temperatures.

A comparison between Eqs. (14) and (15) reveals that the use of the macroscopic hyperbolic heat conduction model is possible if

$$M \approx 1 \tag{20}$$

It will be assumed that if condition in Eq. (20) is satisfied within a 1% deviation, then the macroscopic hyperbolic heat conduction model is satisfied. In this case, $T_e \approx T_l \approx T$ and Eqs. (1) to (3) become

$$(C_e + C_l)\frac{\partial T}{\partial t} = -\frac{\partial q}{\partial x} \tag{21}$$

$$\tau \frac{\partial q}{\partial t} + k\frac{\partial T_e}{\partial x} + q = 0 \tag{22}$$

which is the classical macroscopic hyperbolic heat conduction model. If the deviation in Eq. (20) is more than 1%, then the use of the microscopic hyperbolic heat conduction model is essential. To validate the usage of the macroscopic hyperbolic heat conduction model in layers exposed to a harmonic fluctuating boundary heating source, Eqs. (18)–(20) imply that, with less than 1% deviation between the macroscopic and the microscopic models, then

$$\frac{\omega}{C_R A} < 0.1 \tag{23}$$

In terms of the dimensional properties, Eq. (23) is rewritten as

$$\frac{\bar{\omega} C_l}{G} < 0.1 \tag{24}$$

The criterion in Eq. (24) implies that the macroscopic hyperbolic heat conduction model under the effect of a fluctuating boundary heating source may be used in applications having small frequencies $\bar{\omega}$, small lattice thermal capacity C_l, and large coupling factors G.

Fluctuating heating sources with small frequencies gives the electron gas enough time to transmit its high energy to the solid lattice. Small lattice thermal capacity implies that solid lattice needs small energy to attain the same temperature as the electron gas and, this in turn, shortens the time required by both the lattice and the electron to attain the thermal equilibrium state. Large coupling factor G enhances the energy exchange process between the electron gas and solid lattice, and this also shortens the time required by both to attain the thermal equilibrium state.

The criterion in Eq. (24) reveals that other slab properties such as the film thickness L, relaxation time τ_F, electron-gas thermal conductivity k_e, and electron-gas thermal capacity C_e do not play any role in controlling the state of thermal equilibrium or the necessity of transition from the macroscopic model to the microscopic one.

Table I. Angular Frequencies Beyond Which The Use of The Microscopic Model Is Essential

Metal	$\bar{\omega} \geqslant (\text{rad} \cdot \text{s}^{-1})$
Cu	1.4×10^9
Ag	1.12×10^9
Pb	8.27×10^9

Table I shows the ranges of angular frequency $\bar{\omega}$ beyond which the use of the microscopic heat conduction model is essential in metallic slabs made of different metals.

3. RESULTS AND DISCUSSION

Figures 1 to 4 show the spatial and temporal temperature distributions for the electron gas and the solid lattice, respectively, while Figs. 5 and 6 show the heat flux spatial and temporal distributions. It is clear from these figures that fluctuations in temperature and heat flux disappear as we move far from the boundary. This implies that there is a limited thermal penetration depth for the fluctuating boundary-heating source. Comparing Figs. 1 and 2 with 3 and 4 reveals that the boundary thermal effect has a thicker thermal penetration depth in the electron gas than in the solid lattice. This penetration depth depends on the intensity of the boundary heating source, measured by ε in this case, and on the slab thermal properties combined by the dimensionless groups C_R, A, and ω. Also, Figs. 1 to 6

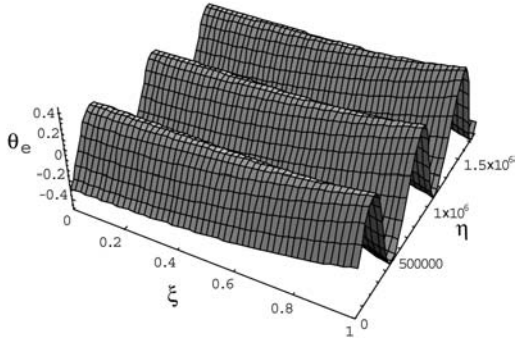

Fig. 1. Spatial and transient electron-gas temperature distribution for Cu ($A = 0.06857$, $B = 0.000551$, $\omega = 0.00001$).

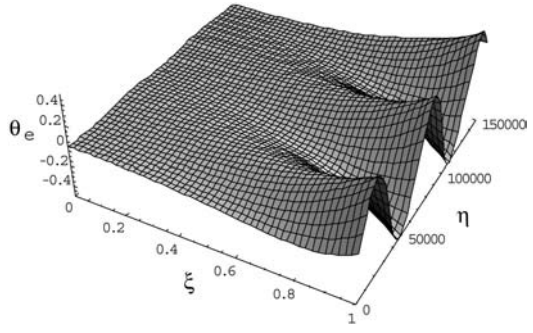

Fig. 2. Spatial and transient electron-gas temperature distribution for Cu ($A = 0.06857$, $B = 0.000551$, $\omega = 0.001$).

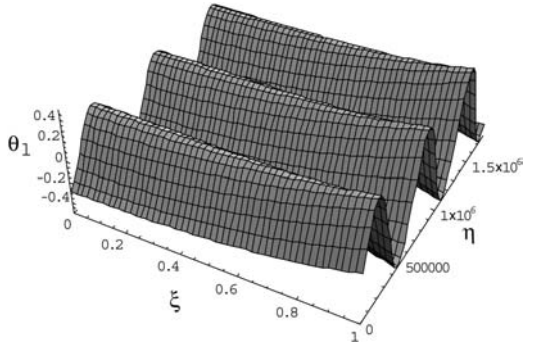

Fig. 3. Spatial and transient solid-lattice temperature distribution for Cu ($A = 0.06857$, $B = 0.000551$, $\omega = 0.00001$).

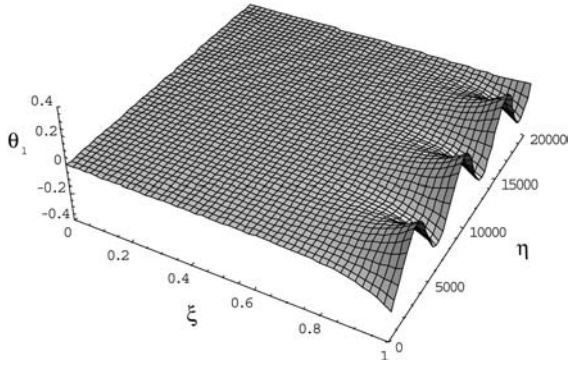

Fig. 4. Spatial and transient solid-lattice temperature distribution for Cu ($A = 0.06857$, $B = 0.000551$, $\omega = 0.001$).

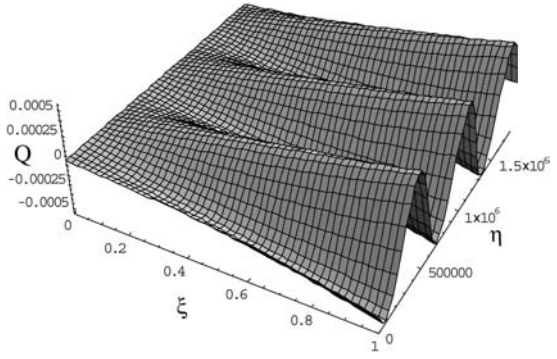

Fig. 5. Spatial and transient dimensionless heat flux distribution for Cu ($A = 0.06857$, $B = 0.000551$, $\omega = 0.00001$).

show that the thermal penetration depth increases as ω decreases. This is due to the fact that the total energy transmitted from the fluctuating heating source to the plate decreases as the frequency of the fluctuating boundary heating source increases. As the frequency of the heating source increases, locations far away from the boundary do not have enough time to feel the variation in the thermal disturbances created at the boundary.

Figures 7 to 9 show the harmonic variation in both electron-gas and solid-lattice temperatures for Cu at different frequencies. As seen from Figs. 7 to 9 the deviation between θ_e and θ_l becomes significant when $\omega > 1 \times 10^{-5}$. Taking into account that most metals have $\tau_F \sim 10^{-14}\, s$, then $\bar{\omega} = \frac{\omega}{\tau_F} = 10^9\, s$. This agrees very well with the predictions of the previous theoretical analysis carried out using an order of magnitude analysis, and summarized in Table I.

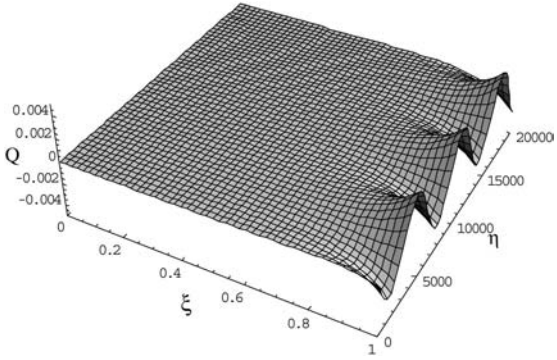

Fig. 6. Spatial and transient dimensionless heat flux distribution for Cu ($A = 0.06857$, $B = 0.000551$, $\omega = 0.001$).

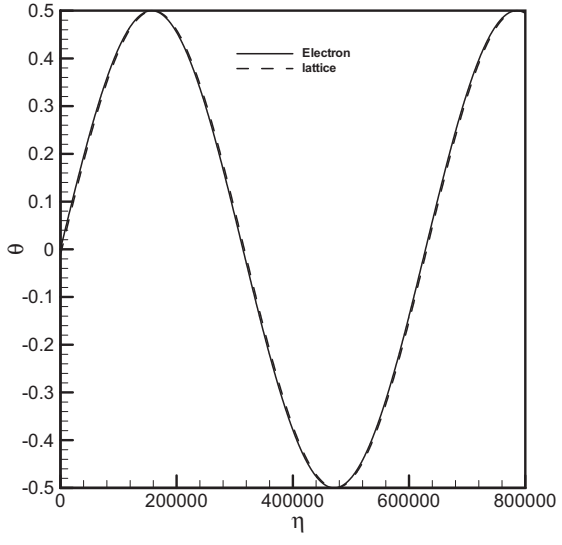

Fig. 7. Transient electron-gas and solid-lattice temperature distributions for Cu ($A = 0.06857$, $B = 0.000551$, $\omega = 0.00001$, $\zeta = 1.0$).

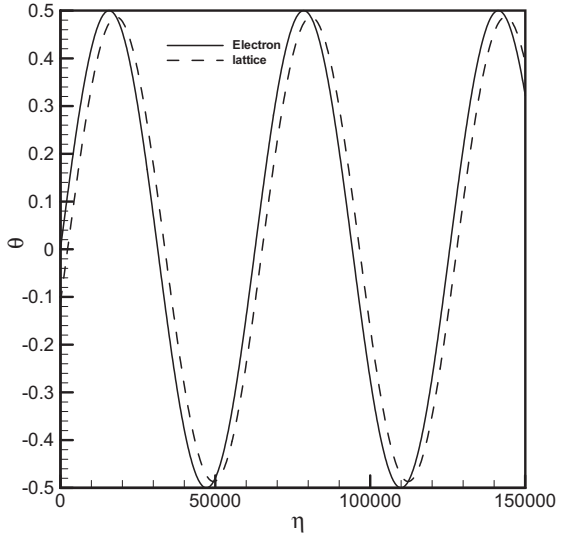

Fig. 8. Transient electron-gas and solid-lattice temperature distributions for Cu ($A = 0.06857$, $B = 0.000551$, $\omega = 0.0001$, $\zeta = 1.0$).

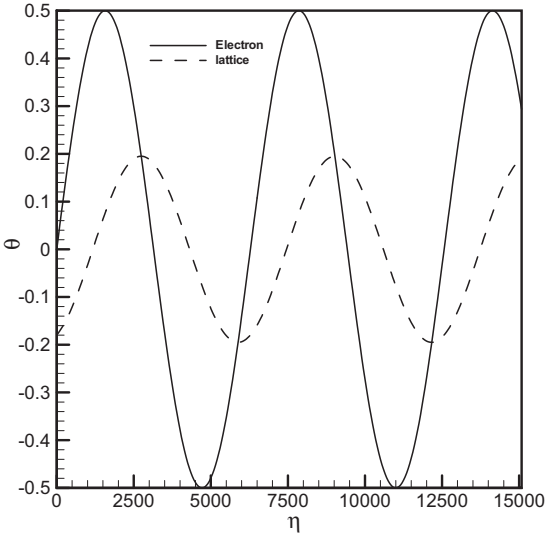

Fig. 9. Transient electron-gas and solid-lattice temperature distributions for Cu ($A = 0.06857$, $B = 0.000551$, $\omega = 0.001$, $\zeta = 1.0$).

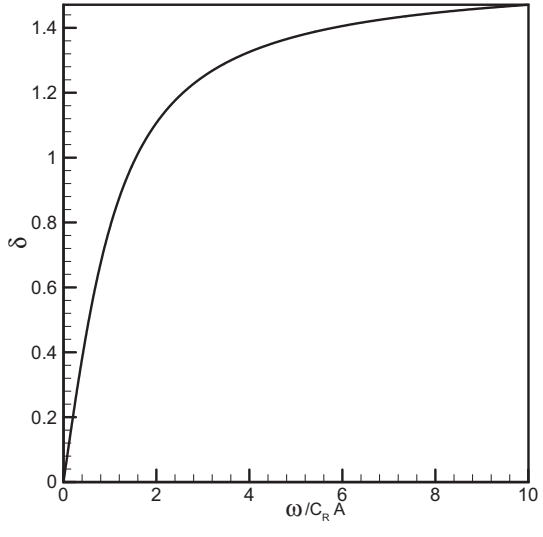

Fig. 10. Variation of the phase shift between the electron-gas and solid-lattice temperature as a function of ω.

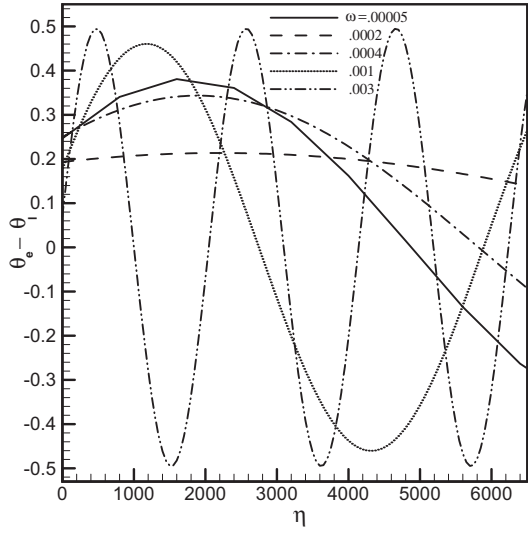

Fig. 11. Transient behavior of the temperature differences $\theta_e - \theta_l$ at different ω for Cu ($A = 0.06857$, $B = 0.000551$, $\zeta = 1.0$).

The phase shift δ as described by Eq. (19) is plotted in Fig. 10 as a function of $\frac{\omega}{C_R A}$. An increase in $\frac{\omega}{C_R A}$ within its lower range leads to a sharp increase in δ. However, this increase becomes slower as $\frac{\omega}{C_R A}$ increases and then δ reaches to an asymptotic value of 1.5708 rad.

As mentioned previously, the group $\frac{\omega}{C_R A}$ represents $\frac{\bar{\omega} C_l}{G}$ on a dimensional basis. It is clear that the phase shift becomes small as $\bar{\omega}$ and C_l decrease and as G increases. Any parameter that shortens the time required by the lattice to exchange energy with the electron gas leads to a reduction $|\theta_e - \theta_l|$ in the phase shift between the electron-gas and the solid-lattice temperatures.

The deviation between electron-gas and solid-lattice temperatures as a function of η is shown in Fig. 11 for Cu. The figure shows that the deviation becomes significant for $\bar{\omega} > 1 \times 10^9$ rad $\cdot$ s^{-1} and is in a good agreement with the predictions of Table I.

4. CONCLUSION

The validity of using the microscopic hyperbolic heat conduction model under the effect of a high frequency fluctuating boundary heating source is investigated. It is found that the microscopic hyperbolic heat conduction model must be used if $\frac{\omega}{C_R A} > 0.1$ on a dimensionless basis or $\frac{\bar{\omega} C_l}{G} > 0.1$ on a dimensional basis. For $\frac{\bar{\omega} C_l}{G} < 0.1$, the difference and the phase

shift between θ_e and θ_l may be neglected and one may assume that $\theta_e \approx \theta_l$. The phase shift between the electron-gas and the solid-lattice temperatures is found to be $\tan^{-1}(\frac{\omega}{C_R A})$. This phase shift reaches a fixed value of 1.5708 rad at very large values of $\frac{\omega}{C_R A}$ or $\frac{\bar{\omega} C_l}{G}$. Regarding the frequency $\bar{\omega}$, it is found that the use of the microscopic hyperbolic heat conduction model is essential when $\bar{\omega} > 1 \times 10^9$ rad $\cdot$ s^{-1} for most metallic films independent of the layer thickness and other thermal properties such as τ_F, k_e, and C_e.

NOMENCLATURE

A	Dimensionless quantity, $G\tau_F / C_e$
B	Dimensionless quantity, $k_e \tau_F / (L^2 C_e)$
C	Heat capacity, J $\cdot$ m^{-3} $\cdot$ K^{-1}
C_R	Heat capacity ratio, C_e / C_l
$E(\zeta)$	Spatial amplitude of the heat flux
G	Electron-phonon coupling factor, W $\cdot$ m^{-3} $\cdot$ K^{-1}
i	Imaginary number, $\sqrt{-1}$
k_e	Electron gas thermal conductivity, W $\cdot$ m^{-3} $\cdot$ K^{-1}
$2L$	Film thickness, m
q	Heat flux, W $\cdot$ m^{-2}
Q	Dimensionless heat flux, $q\tau_F / (LC_e T_o)$
t	Time, s
T	Temperature, K
T_o	Amplitude of harmonic fluctuating temperature, K
$W(\zeta)$	Spatial amplitude of the temperature
x	Transverse coordinate, m

Greek Symbols

ε	Relative amplitude of oscillations
η	Dimensionless time, t/τ_F
θ	Dimensionless temperature, $(T - T_o / T_o)$
τ_F	Relaxation time evaluated at the Fermi surface, s
ζ	Dimensionless axial coordinate, x/L
$\bar{\omega}$	Angular velocity of fluctuating temperature, rad $\cdot$ s^{-1}
ω	Dimensionless angular velocity of fluctuating temperature, $\bar{\omega}\tau_F$

Subscripts

e	Electron gas
l	Solid lattice
R	Ratio

REFERENCES

1. D. Y. Tzou, in *Macro-to-Microscale Heat Transfer—The Lagging Behaviour* (Taylor and Francis, New York, 1997), pp. 1–64.
2. T. Q. Qio and C. L. Tien, *Int. J. Heat Mass Transfer* **35**:719 (1992).
3. T. Q. Qio and C. L. Tien, *ASME J. Heat Transfer* **115**:835 (1993).
4. S. L. Anisimov, B. L. Kapeliovich, and T. L. Perelman, *Sov. Phys. JETP* **39**:375 (1974).
5. J. G. Fujimoto, J. M. Liu, and E. P. Ippen, *Phys. Rev. Lett.* **53**:1837 (1984).
6. D. Y. Tzou, *J. Heat Transfer* **117**:8 (1995).
7. M. A. Al-Nimr and V. S. Arpaci, *Int. J. Heat Mass Transfer* **43**:2021 (2000).
8. M. A. Al-Nimr and V. S. Arpaci, *J. Appl. Phys.* **85**:2517 (1999).
9. M. A. Al-Nimr and S. Masoud, *ASME J. Heat Transfer* **119**:188 (1997).
10. M. A. Al-Nimr, *Int. J. Thermophys.* **18**:1257 (1997).
11. M. A. Al-Nimr, O. M. Haddad, and V. S. Arpaci, *Heat and Mass Transfer* **35**:459 (1999).
12. T. Q. Qiu and C. L. Tien, *Int. J. Heat Mass Transfer* **37**:2789 (1994).
13. S. Kumar and M. Mitra, *Adv. Heat Transfer* **33**:287 (1999).
14. M. A. Al-Nimr and S. Kiwan, *Int. J. Heat Mass Transfer* **44**:1013 (2001).
15. S. Kiwan and M. A. Al-Nimr, *Jpn. J. Appl. Phys.* **39**:4245 (2000).